High Strength and Fatigue Resistant Welds in NiTi and Brass by Impact Welding

Jianxiong Li (li.8266@osu.edu)
The Ohio State University
Boyd Panton
The Ohio State University
Yu Mao
The Ohio State University
Anupam Vivek
The Ohio State University
Glenn Daehn
The Ohio State University

Research Article

Keywords: Vaporizing foil actuator welding, NiTi shape memory alloy, Brass alloy, Pseudoelastic response, Joint efficiency, Dissimilar welding

Posted Date: October 19th, 2021

DOI: https://doi.org/10.21203/rs.3.rs-973576/v1

Abstract

Vaporizing foil actuator welding (VFAW) was used to create high strength and fatigue resistant dissimilar welds between NiTi and a brass alloy for the first time. VFAW uses the high pressure resulting from a vaporized aluminum foil to impact weld NiTi to brass. Advanced techniques were used to characterize the structure, mechanical and functional properties of these impact welds. The results show that NiTi/brass welds had solid-state wavy interfaces with no thermally induced defects. The adjoining area of the interfaces were strengthened compared to the base metals. Martensitic transformation temperature ranges were widened in these dissimilar impact welds. Lap shear tests show that the dissimilar NiTi impact welds exhibited a similar pseudoelastic plateau and maximum stress as the NiTi base metal. The resultant joint efficiencies were near 100 % compared to less than 50 % in traditional welding technologies. Cycling tests show that the NiTi/brass impact welds exhibited very similar pseudoelastic responses as the NiTi base metal with less than 0.5 % irrecoverable strains. Dissimilar impact welding of NiTi to brass provides stronger joining and more design flexibility compared to mechanical crimping, positioning the technology to be a solution to producing high strength actuators and sensors.

1. Introduction:

NiTi shape memory alloys are used as lightweight electro-magnetic actuators in a range of industries including automotive and electronics, due to their large stresses and high recovery strains generated through solid-state operation [1]. The widespread success of NiTi actuators has required the engineering of a suitable design that incorporates numerous material properties including functional stability, higher phase transformation temperatures, a suitable structural fatigue life, smart control systems, and cost reduction. The predominant method to assemble SMA actuators is currently to mechanically fasten or crimp the wire to electrical and mechanical connections. Crimping results in minimal mechanical and no thermal changes to the SMA, leading to fatigue lives in the millions of cycles. Issues with mechanical fastening and crimping include low pull-out strength, increase in size and weight, stress concentrations, significant design input required to achieve reliable joints as well as low mechanical stability and reliability and limited accommodation of nonstandard geometries. A metallurgically joint of NiTi to a traditional alloy such as copper-based alloys would potentially have overcome some of the limitations associated with mechanical joining technologies [2, 3]. Candidates for these joints for actuators including stainless steel, copper, and brass.

Fusion welding of NiTi to Cu shows several issues such as the formation of heat affected zones and brittle intermetallics including CuTi, Cu_4Ti_3 and Cu_2Ti [3]. Laser welding is by far the most researched method for NiTi dissimilar welding due to its precision, small heat affected and fusion zones, and minimal residual stresses and distortion [4]. However, this method still involves degradation of mechanical and functional properties due to the formation of brittle intermetallics and thermally induced defects caused by the melting and solidification of base metals.

Solid state welding methods are preferable since there are no large-scale melting or distortion occurred in the welds. These methods minimize large amounts of thermally induced defects which are common in fusion-based welding. Rotational friction welding has been used by Integer Medical however the joint geometry is unsuitable for actuation, and research in the area shows issues with small process windows [5–7].

Ultrasonic welding relies on the ultrasonic vibration to break down the surface oxides and asperities to achieve a metallurgical bonding. This method is characteristic of lower heat input and short welding cycles compared to other welding approaches [8, 9]. Zhang et al. studied the ultrasonic spot welding of NiTi to copper to NiTi where copper was used as an interlayer [10]. The results show that a nanoscale transition layer was formed between NiTi and Cu which improves the mechanical performance of NiTi welds. Ultrasonic welding is, however, limited to thin foils. The large indentations or even fracture left on the top surface of the base metals could also limit its use in the actuator industry.

Impact welding methods such as vaporizing foil actuator welding (VFAW) has been shown to be extremely versatile and efficient in joining dissimilar metal alloys including Al/Fe [11], Ti/stainless steel[12], and NiTi/stainless steel [13, 14]. This method relies on the decomposition of an aluminum foil which generates an intense plasma to drive one piece of metal (flyer) towards another piece (target) and form a solid-state impact weld. This method forms little to no HAZ and retains full strength of the base metals in the impact welds.

In the current article the authors investigate how VFAW can be used to join NiTi and brass alloys for the first time. The dissimilar impact welds between NiTi and brass were compared with traditional NiTi mechanical ring type crimps in terms of maximum pullout force and design flexibility. The microstructure, phase transformation characteristics, microhardness distributions, and mechanical and functional properties of the NiTi/brass impact welds were studied.

2. Materials And Methods:

464 brass sheets (59Cu-40Zn-1Sn) with dimensions of 40 mm by 60 mm by 1mm were selected as the flyer material. NiTi SMA round wires with diameter of 0.762 mm, provided by Fort Wayne Metals, were chosen as the target material. Polycarbonate plastic sheets were used as impact resistant sheets (Fig. 1b). The energy source used in this work was a Magneform capacitor bank with maximum energy of 16 kJ, a total capacitance of 426 μF, an inductance of 100 nH, and a rise time of 12 μs. The input energy was optimized to be 12 kJ for all samples. Fig. 1 shows the schematic representation of the VFAW process to weld the brass sheet to NiTi wire. A 0.076 mm thick spot type foil was placed beneath and insulated from the brass sheet flyer (Fig. 1a), which will be vaporized after discharging the energy from the capacitor bank. This type of foil will generate an impact velocity of 600-700 m/s under an input energy of 12 kJ [15]. Two plastic standoff sheets with thickness of 2.4 mm and separation distance of 20 mm were used to provide the necessary acceleration distance and impact angle for achieving impact welds (Fig. 1c). The patch VFAW process has been described in detail in a previous work [16]. However, this work

presents a different target format. Due to the round shape of the NiTi wire, two impact resistant sheets with matched dimensions were placed besides the target wire to achieve a flat impact surface (Fig. 1b). In VFAW process, a high current on the range of 100 kA goes through the aluminum foil, the narrowest area of the foil will vaporize rapidly and create a high pressure plasma (2-12 GPa) [17]. This high pressure plasma drives the brass flyer through the standoff distance towards the target and forms a collision weld.

After welding, the NiTi/Brass welds were cut, cross-sectioned, and polished down to 1 μm with diamond paste. The interfacial microstructures were characterized through optical microscopy (OM) and scanning electron microscopy (SEM) equipped with energy-dispersive x-ray spectroscopy (EDS). The phase transformation characteristics of NiTi wire BM and NiTi/Brass welds were measured by differential scanning calorimetry (DSC) using a DSC2500 calorimeter made by TA instruments. The DSC measurements were conducted at temperatures ranging from -80 to 120 °C under an Argon atmosphere. The controlled heating and cooling rates are 10 °C/min. DSC samples were prepared with a weight of 10-17 mg for the NiTi wire BM and NiTi/Brass welds. All the DSC procedures follow the ASTM F2004-17 standard. Microhardness distributions across the NiTi/Brass weld interfaces were measured with a square-based pyramid diamond indenter operating at a load of 300 g and a dwell time of 15 s.

Fig. 2 shows the schematic representations of the mechanical testing setups for NiTi BM and NiTi/Brass welds. The NiTi BM was tested at a gauge length of 50 mm (Fig. 2b). While the NiTi/Brass welds were tested at the same gauge length of 50 mm, the displacement observed is a composite of weld region and remaining NiTi and brass base metals due to the deformation of both regions during tests. Displacement was measured with the Linear Variable Differential Transformer (LVDT) in the test-frame base. Because of this and the straightening of the NiTi/Brass welds on initial loading, displacements cannot be accurately related to strains. Lap shear tests were conducted on an MTS EM Test Frame with a displacement rate of 1 mm/min for NiTi base metal and NiTi/Brass dissimilar welds. Three replicates were tested for each type of the samples. The cycling tests with a limited number of 500 cycles were performed with displacement control from 0 to 2 mm and load control down to 0 N under a crosshead displacement rate of 0.02 mm. min^{-1}. mm^{-1} based on ASTM F2516-18 standard. The displacement rate for cycling tests is calculated as 1 mm/min and the cycling strain is 4 % for all samples.

3. Results And Discussion:

3.1. Macro appearance and comparison to traditional crimps

VFAW produces a NiTi wire/Brass sheet weld with little plastic deformation on the brass side except the wire/sheet welding area (Fig. 3b). After being machined to a similar ring shape (Fig. 3c), the NiTi/Brass weld can be used to simulate or replace a traditional ring type mechanical crimp (Fig. 3a). Current work is underway to weld directly to a crimp. The traditional ring type mechanical crimp presents a maximum pull-out force as low as 140 N [1, 18]. This is much lower than the peak load of the NiTi/Brass impact weld (640 N) which was shown in Fig. 7. This proves that VFAW can be used to produce NiTi actuators

with higher strength connection between the NiTi wire and a structural part compared to mechanical crimping method.

3.2. Interfacial microstructures

To reveal the interfacial bonding quality and mechanism, detailed microstructure characterizations were conducted on a typical NiTi/Brass weld cross-section (Fig. 4). Wavy structures with little macro-defects were observed in the NiTi/Brass weld interface (Fig. 4a), which is characteristic of VFAW [19]. The hook-shape gaps on both sides of the NiTi/Brass weld are caused by the high strain rate plastic deformation during the VFAW process. This high strain rate plastic deformation drives the brass alloy to flow upward along the circumferential direction of the NiTi wire. A magnified view of the wavy interface exhibited a solid-state defect-free metallurgical bonding between the NiTi and brass alloy (Fig. 4b). This was verified by the EDS mapping analyses shown in Fig. 4c, d, e, and f which exhibited sharp transitions between the major elements in NiTi (Ni and Ti) and those in brass alloy (Cu and Zn).

3.3. Phase transformation characteristics

Phase transformation behaviors of NiTi SMA subjected to impact welding are good indicators of the functional properties of NiTi dissimilar welds. Fig. 5 compares the DSC results of the NiTi BM and a typical NiTi/Brass weld. Transformation temperatures, thermal hysteresis and enthalpies of both types of samples are summarized in Table 1. Phase transformation temperatures such as M_s, M_f, R_s, R_f, A_s and A_f were determined through the intersection of the baseline with the line of maximum inclination of the transformation peaks based on the ASTM F2004-17 standard. Thermal hysteresis () was determined by the difference between the peak temperatures. Enthalpies were calculated by integrating the peak areas over the baseline (time).

Thermal hysteresis and enthalpies can be used to examine the extent of phase transformation. It was reported that a complete reversible B2 to B19’ transformation generally exhibits a thermal hysteresis ranging from 35 to 50 °C and enthalpies ranging from 10 to 25 J g^{-1}, respectively [20, 21]. In the current work, the calculated thermal hysteresis and enthalpies for NiTi BM are lower than 10 J g^{-1} and 10 °C, respectively. This shows that only intermediate B2-R reversible transformation occurred in the NiTi base metal. This intermediate phase transformation is possibly due to the presence of precipitates and nanocrystalline grains in the NiTi BM caused by the thermo-mechanical processing. The transformation temperatures, thermal hysteresis and enthalpies for the NiTi/Brass welds cannot be determined due to the lack of apparent heat flow peaks. It was also shown that the phase transformation temperature ranges of the NiTi/Brass welds are widened compared to that in the NiTi BM.

The martensitic transformation was shown to be significantly suppressed in both NiTi BM and the NiTi/Brass weld, while the latter is more severe. For the NiTi BM, the nanocrystalline grains and precipitates restrict the structure and make the martensitic transformation difficult. The large heterogeneity in internal stresses increases the barrier to complete phase transformation. For the NiTi/Brass weld, apart from the microstructure constriction brought by the NiTi BM, the high strain rate

plastic deformation in the VFAW process will further increase the barrier to transformation [22, 23]. The thermal mass of the inactive brass alloy likely impedes the phase transformation to a large extent. There may have been limited phase transformation in the NiTi but it was below the detection limits of the DSC system [24]. These all explain why there are no heat flow peaks in the NiTi/Brass weld.

The readings could also have been affected by the thermal mass of brass in the DSC test. Suppression of the phase transformation was limited to the immediate joint area, and is posited as a potential benefit. A gradient in transformation properties may serve to reduce plastic strain buildup as opposed to a step-wise change at the interface between NiTi and brass.

Table 1. Transformation temperatures (°C), thermal hysteresis (), and enthalpies () of the NiTi base metal and NiTi/Brass weld where and indicate the austenite start and finish temperatures, respectively; and indicate the R phase start and finish temperatures, respectively; and indicate the martensite start and finish temperatures, respectively.

Samples	Transformation temperatures (°C)						(°C)	($J\ g^{-1}$) Cooling	Heating
NiTi BM	-1.95	24.6	23	-11.7	-	-	6.44	5.61	4.62
NiTi/Brass weld	-	-	-	-	-	-	-	-	-

3.4. Mechanical properties

3.4.1. Microhardness distributions

To reveal the mechanical behavior of the NiTi/Brass weld, microhardness distributions across the welding interface were examined. Three different progressions (top, middle and bottom) from the brass alloy to the NiTi side were carried out perpendicular to the welding interface (Fig. 6a). It is worthwhile to mention that the hardness measurements on the NiTi side might not be as quantitatively accurate as those on the brass alloy side due to the partial recovery caused by stress induced martensitic transformation.

The results show that the area near the NiTi/Brass interface gained 15.6% increase of hardness compared to the brass alloy base metal while the area near the NiTi side exhibited comparable hardness distributions as the NiTi BM. These measurement results confirm that little or no heat affected zones were formed in the NiTi/Brass impact welds. This has been observed in VFAW of other metal combinations such as NiTi/Stainless steel (SS) [24, 25] and Ti/SS [12]. The lack of HAZ formation is an advantage over other traditional fusion-based and solid-state welding technologies normally involving thermal softening. The improved strength of the welding interface is likely caused by the grain refinement in the adjoining areas induced by the high strain rate plastic deformation in the VFAW process [26].

3.4.2. Lap shear test results and joint efficiency

Lap shear tests were performed on the NiTi BM and NiTi/Brass welds to compare the mechanical strength and ductility of samples before and after welding. Fig. 7 shows the load-displacement curves of

the NiTi BM and a typical NiTi/Brass weld. Note that the nominal stress is calculated through dividing the load by the cross-section area of the NiTi BM wire, and the nominal strain is the ratio of crosshead displacement to the gauge length. It was observed that the stress-strain curve of the NiTi/Brass weld exhibited a relatively larger elastic slope compared to that in the NiTi BM. This difference in elastic slope is due to the lap joint morphology of the NiTi/Brass weld causing rotation of the sample. The stress plateau of the NiTi/Brass weld is narrower and more inclined in comparison with that of the NiTi BM due to half of the gauge length being brass alloy. Note that the stress plateau is caused by the transformation of austenite to a variant of martensite predetermined by the applied stress direction [27]. During the plateau stage a certain amount of strain can be accommodated while exceeding a threshold value, plastic deformation will occur. The plastic deformation of brass alloy would cause more rapid shifting of stress and strain towards the elastic-plastic stage. The peak stress of the NiTi/Brass weld is around 97% of the ultimate tensile strength (UTS) of the NiTi BM.

In this work, the ratio of peak stress of the weld to the UTS of the NiTi BM is used as a reference to compare the joint efficiencies among varied joint technologies. Table 2 compares the joint efficiencies and main issues/microstructures for failure of the NiTi/Cu dissimilar welds made by laser welding (LSW) and ultrasonic spot welding (USW), as well as NiTi/Brass welds made by VFAW in the current work. Detailed welding design data including material type, weld format, and base metal dimensions were also provided for good comparisons.

It was observed that NiTi/Cu welds made by LSW exhibited joint efficiency lower than 60 % due to grain growth, microstructure softening as well as the formation of Cu-based or $Ni_xTi_yCu_z$ IMC [2, 3, 28, 29]. NiTi/Cu/NiTi welds made by USW entail higher joint efficiencies ranging from 60 to 86% [10, 30]. The relatively higher joint efficiencies compared to those made by LSW are due to the solid-state welding nature of USW which relies on friction and plastic deformation. The friction and plastic deformation break the oxide layers and form mechanical interlocking and direct metallurgical bonding between NiTi and Cu. It should be noted that this process is limited to use with very thin foils (e.g. <150μm). The NiTi/Brass welds made by VFAW in the current work exhibited the highest joint efficiency. One of the reasons is that impact welding is a solid-state welding method which minimizes or avoids large scale melting of the base metals. No thermally induced defects including grain growth or brittle $Ni_xTi_yCu_z$ IMC formed in these welds. The second reason is that during the VFAW process, the high velocity jetting scours away the possible oxides and achieves a nascent surface for metallurgical bonding [24]; compared to USA which will retain oxides in the interface of welds [10]. The lack of HAZ formation, the strengthened interface due to grain refinement (Fig. 6), and no oxide segregation on the interface all contribute to the high strength NiTi/Brass impact welds.

Table 2. Comparison of joint efficiency (weld strength/UTS of the NiTi base metal) and main issues/microstures for failure of NiTi/Cu dissimilar welds made by laser welding and ultrasonic spot welding, as well as NiTi/Brass welds made by VFAW in this work.

Method	Joint efficiency	Material type	Weld format	Base metal dimensions	Microstructures for failure	Failure locations	References
LSW-1	17.1%	NiTi/Cu wires	Butt	D=400 μm	Grain growth and softening	Cu BM	[28]
LSW-2	53.6%	NiTi wire/Cu sheet	Lap	D_{NiTi}= 700 μm; 2.0 × 25.0 × 0.5 mm	Cu-based IMC	FZ	[2]
LSW-3	38.3%	NiTi wire/Cu sheet	Lap	D_{NiTi}= 700 μm; 2.0 × 25.0 × 0.5 mm	NiTiCu IMC; equiaxed and lamellar regions; Islands of copper	Cross-section of the joint	[3]
LSW-4	18.7%	NiTi/Cu wires	Butt	D=400 μm	Columnar dendritic Microstructures; $Ni_xTi_yCu_z$ IMC	Cu HAZ	[29]
USW-1	64.2%	NiTi sheet/Cu foil/NiTi sheet	Lap	t_{NiTi}= 150 μm; t_{Cu}=20 μm	Mechanical interlocking and metallurgical adhesion	Weld interface	[30]
USW-2	85.6%	NiTi sheet/Cu foil/NiTi sheet	Lap	NiTi (60 × 15 × 0.2 mm); t_{Cu}=100 μm	Nano-scale transition layer composed of NiTiCu phase	NiTi BM	[10]
VFAW	97%	NiTi wire/Brass sheet	Lap	D_{NiTi}=0.762 mm; 40 × 60 × 1 mm	Mechanical interlocking and metallurgical adhesion	NiTi BM	Current work

3.4.3. Cycling tests

The typical applications of NiTi alloys such as actuators generally involves many loading and unloading cycles during the motion control process. Apart from the high joint strengths presented by the lap shear tests, the functional fatigue property of the samples is also important. 500 stress-strain cycles were conducted on both the NiTi BM and NiTi/Brass welds to determine the superelastic behavior and functional stability (Fig. 8). The 1^{st}, 100^{th}, 200^{th}, 300^{th}, 400^{th}, and 500^{th} cycles were singled out to better reflect the stabilization of pseudoelastic plateaus and the accumulation of irrecoverable strains during the cycling tests. Future work is focused on characterizing the response of the welds to thermal martensitic cycling.

The superelastic plateaus on the first cycle for the NiTi BM and NiTi/Brass weld occurred at 240 N and 226 N, respectively. The forward superlelastic plateaus on the last cycle of these two samples occurred at 170 N and 150 N, respectively. This means that after 500 cycles, the superelastic plateaus were lowered down by 70 N for all the samples. From 100^{th} to 500^{th} cycles, the superelastic plateaus only decrease by 15 N which means both samples start to stabilize after 100 cycles. The difference in the plateau stress

for the NiTi BM and the NiTi/Brass weld is possibly due to the half gauge length of NiTi/Brass weld being brass alloy which does not exhibit superelastic behavior.

A small stress kink is located ahead of the stress plateau of the NiTi base metal, and such a stress kink usually indicates that a higher stress is required to overcome the barrier at the onset of the stress-induced martensitic transformation (SIMT) [31]. Such stress kink was not observed in the NiTi/Brass weld. This indicates that a lower stress is needed to induce martensitic transformation in the NiTi/Brass welds compared to NiTi BM which corresponds to the results shown in Fig. 8.

As the number of cycles continues, the accumulated irrecoverable strain increases up to a point where the stabilization plateau is reached due to the pile-up of dislocations and other lattice defects induced during the stress induced transformation [32]. NiTi/Brass weld exhibited a high irrecoverable strain (0.42 %) than that of the NiTi BM (0.37 %). The pseudoelastic curve of NiTi BM tends to converge faster than that of the welded joint to the stabilized response, accumulating less irrecoverable strain on each successive cycle. There are three sources for the residual strain: (a) the stabilized R phase; (b) the stabilized martensite in SIMT and (c) plastic deformation [33,34]. These irrecoverable strains are significantly lower than those observed in fusion-based welding methods [33–36]. The melting and solidification that occurred in fusion-based welding methods can form intermetallics and large grains in the fusion zone and HAZ, which contribute to the degradation of functional properties.

It was reported that a lower stress for inducing martensite transformation indicates a better fatigue resistance [37]. A lower barrier to induce the martensite could contribute to a higher fatigue resistance by diluting the stress through local SIMT. Following this logic it is predicted that the fatigue resistance of the NiTi/Brass welds will not be degraded by the VFAW process. Future work is underway to investigate the fatigue resistance of these joints in both mechanical and thermomechanical fatigue.

Conclusion

This work demonstrates high strength and fatigue resistant welds between NiTi and brass alloy produced by an impact welding method. The process, microstructure and mechanical and functional properties of NiTi/Brass dissimilar impact welds have been studied and main conclusions have been drawn as follows:

- Vaporizing foil actuator welding was for the first time used to join NiTi to a brass alloy.
- VFAW can manufacture defect-free high strength welds between NiTi SMA and a brass alloy that are 50% greater strength than current state-of-the-art welding methods and 357% greater strength that industry standard crimping.
- The NiTi/brass impact welds exhibited solid-state wavy interfaces, which is characteristic of impact welding.
- Phase transformation characteristics have been highly suppressed in the weld due to the high strain rate plastic deformation.

- Lap shear test show that NiTi/brass impact welds exhibited much higher joint efficiency (97%) compared to less than 50% in traditional methods. the lack of HAZ formation, the strengthened interface due to grain refinement, and no oxide segregation on the interface all contribute to the high strength NiTi/Brass impact welds.
- The pseudoelasticity of NiTi has been largely preserved after impact welding. The pseudoelastic curve of NiTi BM tends to converge faster than that of the welded joint to the stabilized response, accumulating less irrecoverable strain on each successive cycle. These irrecoverable strains (less than 0.5 %) are significantly lower than those observed in fusion-based welding methods.
- Dissimilar impact welding of NiTi to brass provides stronger joining and more design flexibility compared to mechanical crimping, positioning this technology as a solution to producing high strength actuators and sensors.

Declarations

Author contributions

Jianxiong Li: Conceptualization, Methodology, Data curation, Writing - original draft, Writing - review & editing. **Boyd Panton:** Resources,Methodology, Writing -review & editing, Supervision. **Yu Mao:** Methodology, Data curation. **Anupam Vivek:** Methodology, Supervision**. Glenn Daehn:** Resources, Data curation, Writing - review & editing, Supervision.

Funding

There is currently no funding associated with this project.

Data availability

All data generated or analyzed during this study are included in this published article.

Ethical approval Ethics approval was not required for this research.

Consent to participate Not applicable.

Consent for publication The authors do agree that the copyright of this paper is transferred to Springer's journal "The International Journal of Advanced Manufacturing Technology" when the paper is accepted for publication.

Competing interests The authors declare no competing interests.

References

1. Fumagalli L, Butera F, Coda A (2009) SmartFlex® NiTi wires for shape memory actuators. J Mater Eng Perform 18:691–695. https://doi.org/10.1007/s11665-009-9407-9

2. Zeng Z, Oliveira JP, Yang M et al (2017) Functional fatigue behavior of NiTi-Cu dissimilar laser welds. Mater Des 114:282–287. https://doi.org/10.1016/j.matdes.2016.11.023
3. Zeng Z, Panton B, Oliveira JPP et al (2015) Dissimilar laser welding of NiTi shape memory alloy and copper. Smart Mater Struct 24:125036. https://doi.org/10.1088/0964-1726/24/12/125036
4. Oliveira JP, Fernandes FMB, Miranda RM et al (2016) Residual stress analysis in laser welded NiTi sheets using synchrotron X-ray diffraction. Mater Des 100:180–187. https://doi.org/10.1016/j.matdes.2016.03.137
5. Masayuki Nakamura (1994) Kaisuke Shiroyama; Satoru Masunaga; Kazuo Murata. Method for Joining Parts of Ni-Ti Alloys with Different Metals
6. Gupta PARAHJB (2016) Solid state methods for joining dissimilar metal. guidewire segments without the use of tertiary material
7. Fukumoto S, Inoue T, Mizuno S et al (2010) Friction welding of TiNi alloy to stainless steel using Ni interlayer. Sci Technol Weld Join 15:124–130. https://doi.org/10.1179/136217109X12577814486692
8. Fujii HT, Goto Y, Sato YS, Kokawa H (2016) Microstructure and lap shear strength of the weld interface in ultrasonic welding of Al alloy to stainless steel. Scr Mater 116:135–138. https://doi.org/10.1016/j.scriptamat.2016.02.004
9. Kim J (2014) Weldability of Cu54Zr22Ti18Ni6 bulk metallic glass by ultrasonic welding processing. Mater Lett 130:160–163. https://doi.org/10.1016/j.matlet.2014.05.056
10. Zhang W, Ao S, Oliveira JP et al (2020) On the metallurgical joining mechanism during ultrasonic spot welding of NiTi using a Cu interlayer. Scr Mater 178:414–417. https://doi.org/10.1016/j.scriptamat.2019.12.012
11. Kapil A, Lee T, Vivek A et al (2018) Benchmarking strength and fatigue properties of spot impact welds. J Mater Process Technol 255:219–233. https://doi.org/10.1016/j.jmatprotec.2017.12.012
12. Li J, Vivek A, Daehn G (2021) Improved properties and thermal stability of a titanium-stainless steel solid-state weld with a niobium interlayer. J Mater Sci Technol 79:191–204. https://doi.org/10.1016/j.jmst.2020.11.050
13. Li J, Panton B, Liang S et al (2020) High strength welding of NiTi and stainless steel by impact: Process, structure and properties. Mater Today Commun 25:. https://doi.org/10.1016/j.mtcomm.2020.101306
14. Li J, Panton B, Mao Y et al (2020) High strength impact welding of NiTi and stainless steel wires. Smart Mater Struct. https://doi.org/10.1088/1361-665X/aba847
15. Prasad KS, Mao Y, Vivek A et al (2020) A Rapid Throughput System for Shock and Impact Characterization: Design and Examples in Compaction, Spallation, and Impact Welding. J Manuf Mater Process 4:116
16. Vivek A, Hansen SR, Liu BC, Daehn GS (2013) Vaporizing foil actuator: A tool for collision welding. J Mater Process Technol 213:2304–2311. https://doi.org/10.1016/j.jmatprotec.2013.07.006

17. Nassiri A, Zhang S, Lee T et al (2017) Numerical investigation of CP-Ti & Cu110 impact welding using smoothed particle hydrodynamics and arbitrary Lagrangian-Eulerian methods. J Manuf Process 28:558–564. https://doi.org/10.1016/j.jmapro.2017.04.032
18. Lb L (2009) C R I MP S for SmartFlex ® Wires Barrel Crimp CRIMP Barrel 2 mm Typical delivery packaging Design parameters to order crimped Smartflex. wire Typical Pull-Out Max Force [N]
19. Li J, Schneiderman B, Song S et al (2020) High strength welding of Ti to stainless steel by spot impact: microstructure and weld performance. Int J Adv Manuf Technol 108:1447–1461. https://doi.org/10.1007/s00170-020-05506-4
20. Otsuka K, Wayman-Shape CM Memory Materials-Cambridge University Press (1998) | Shape Memory Alloy | Crystal Structure. https://www.scribd.com/document/368059783/K-Otsuka-C-M-Wayman-Shape-Memory-Materials-Cambridge-University-Press-1998. Accessed 15 Jun 2021
21. Oliveira JP, Barbosa D, Fernandes FMB, Miranda RM (2016) Tungsten inert gas (TIG) welding of Ni-rich NiTi plates: Functional behavior. Smart Mater Struct 25:03LT01. https://doi.org/10.1088/0964-1726/25/3/03LT01
22. Polatidis E, Zotov N, Bischoff E, Mittemeijer EJ (2015) The effect of cyclic tensile loading on the stress-induced transformation mechanism in superelastic NiTi alloys: An in-situ X-ray diffraction study. Scr Mater 100:59–62. https://doi.org/10.1016/j.scriptamat.2014.12.013
23. Delville R, Malard B, Pilch J et al (2010) Microstructure changes during non-conventional heat treatment of thin Ni-Ti wires by pulsed electric current studied by transmission electron microscopy. Acta Mater 58:4503–4515. https://doi.org/10.1016/j.actamat.2010.04.046
24. Li J, Panton B, Mao Y et al (2020) High strength impact welding of NiTi and stainless steel wires. Smart Mater Struct 29:. https://doi.org/10.1088/1361-665X/aba847
25. Li J, Panton B, Liang S et al (2020) High strength welding of NiTi and stainless steel by impact: Process, structure and properties. Mater Today Commun 25:101306. https://doi.org/10.1016/j.mtcomm.2020.101306
26. Agrawal AK, Singh A, Vivek A et al (2018) Extreme twinning and hardening of 316L from a scalable impact process. Mater Lett 225:50–53. https://doi.org/10.1016/j.matlet.2018.04.044
27. Brotzu A, Di Cocco V, Iacoviello F et al (2021) Standards for shape memory alloy applications. In: Shape Memory Alloy Engineering. Elsevier, pp 77–111
28. Sun Q, Chen J, Wang X et al (2021) Study on weld formation and segregation mechanism for dissimilar pulse laser welding of NiTi and Cu wires. Opt Laser Technol 140:107071
29. Shamsolhodaei A, Sun Q, Wang X et al (2020) Effect of Laser Positioning on the Microstructure and Properties of NiTi-Copper Dissimilar Laser Welds. https://doi.org/10.1007/s11665-020-04637-9
30. Zhang W, Ao S, Oliveira JP et al (2018) Microstructural characterization and mechanical behavior of NiTi shape memory alloys ultrasonic joints using Cu interlayer. Materials (Basel) 11:1830. https://doi.org/10.3390/ma11101830
31. Otsuka K, Wayman CM (1987) Shape Memory Materials. Cambridge University Press, Cambridge

32. Miyazaki S, Imai T, Igo Y, Otsuka K (1986) EFFECT OF CYCLIC DEFORMATION ON THE PSEUDOELASTICITY CHARACTERISTICS OF Ti-Ni ALLOYS. Metall Trans A, Phys Metall Mater Sci 17 A:115–120. https://doi.org/10.1007/BF02644447
33. Oliveira JP, Miranda RM, Schell N, Fernandes FMB (2016) High strain and long duration cycling behavior of laser welded NiTi sheets. Int J Fatigue 83:195–200. https://doi.org/10.1016/j.ijfatigue.2015.10.013
34. Chan CW, Man HC, Yue TM (2012) Effect of postweld heat treatment on the microstructure and cyclic deformation behavior of laser-welded niti-shape memory wires. Metall Mater Trans A Phys Metall Mater Sci 43:1956–1965. https://doi.org/10.1007/s11661-011-1062-8
35. Gugel H, Schuermann A, Theisen W (2008) Laser welding of NiTi wires. Mater Sci Eng A 481–482:668–671. https://doi.org/10.1016/j.msea.2006.11.179
36. Hsu YT, Wang YR, Wu SK, Chen C (2001) Effect of CO_2 laser welding on the shape-memory and corrosion characteristics of TiNi alloys. Metall Mater Trans A Phys Metall Mater Sci 32:569–576. https://doi.org/10.1007/s11661-001-0073-2
37. Hornbogen E (2002) Some effects of martensitic transformation on fatigue resistance. Fatigue Fract Eng Mater Struct 25:785–790. https://doi.org/10.1046/j.1460-2695.2002.00579.x

Figures

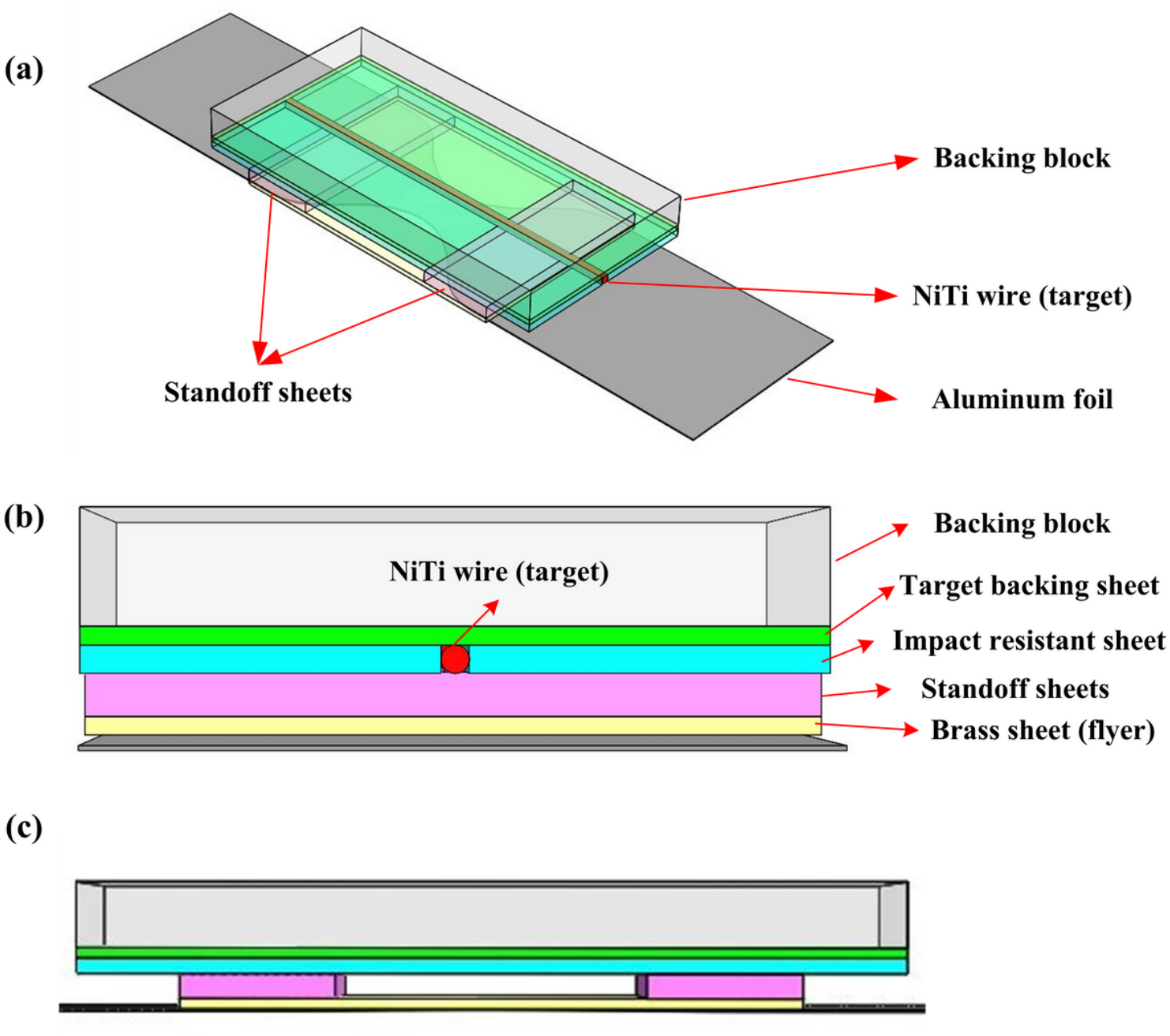

Figure 1

Schematics of experimental setups. (a) Isometric view; (b) Side view; (c) Front view.

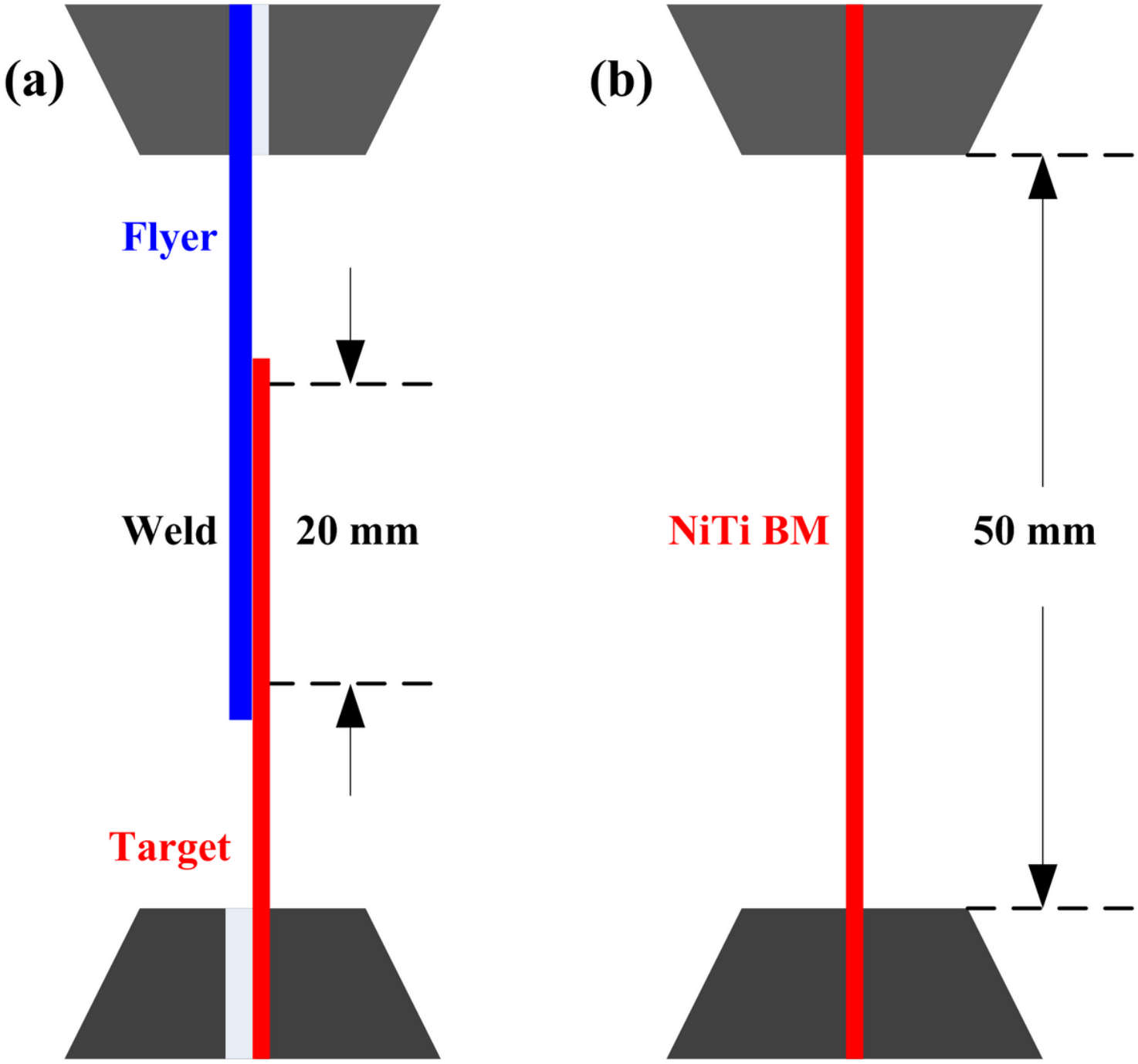

Figure 2

Schematics of mechanical testing setups. (a) Setup for NiTi/Brass weld; (b) Setup for NiTi BM.

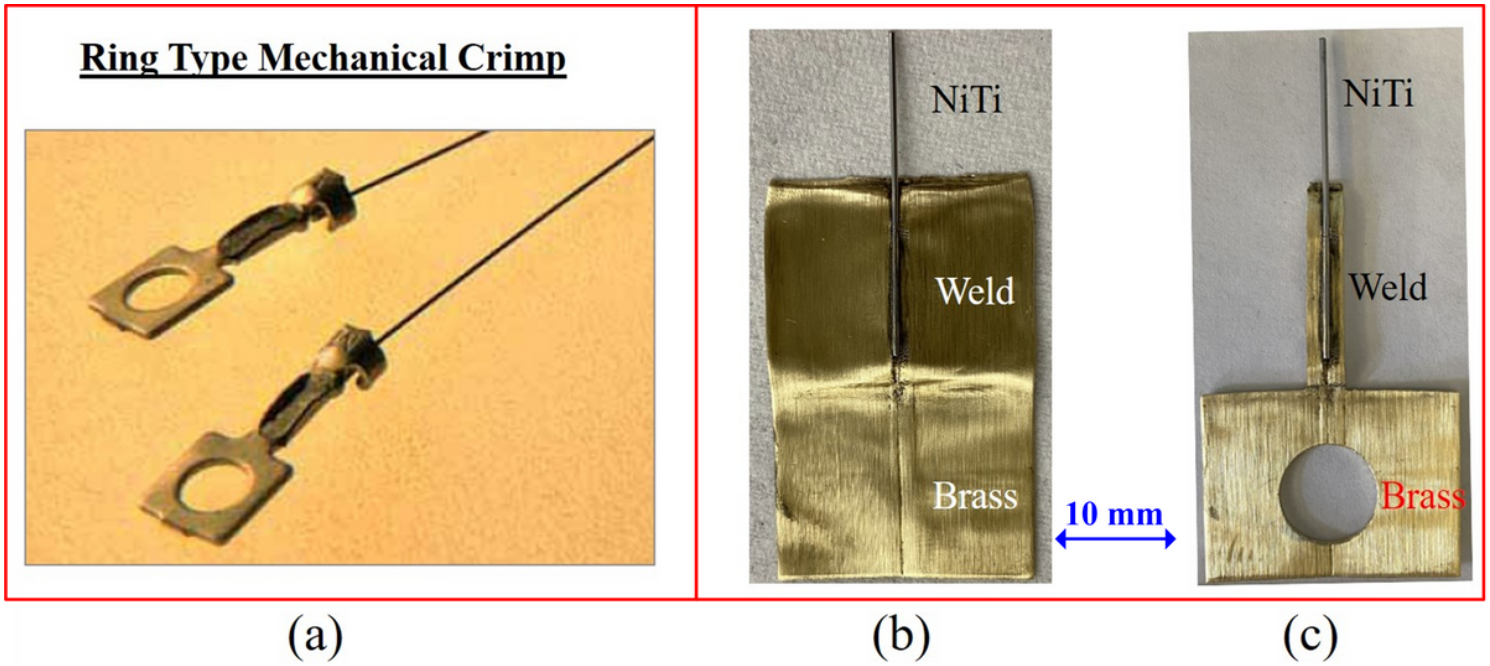

Figure 3

Sample appearances and comparison of traditional ring type mechanical crimp and machined NiTi/Brass weld crimp. (a) Traditional ring type mechanical crimp [1, 18]; (b) NiTi/Brass weld made by VFAW; (c) Machined NiTi/Brass weld crimp.

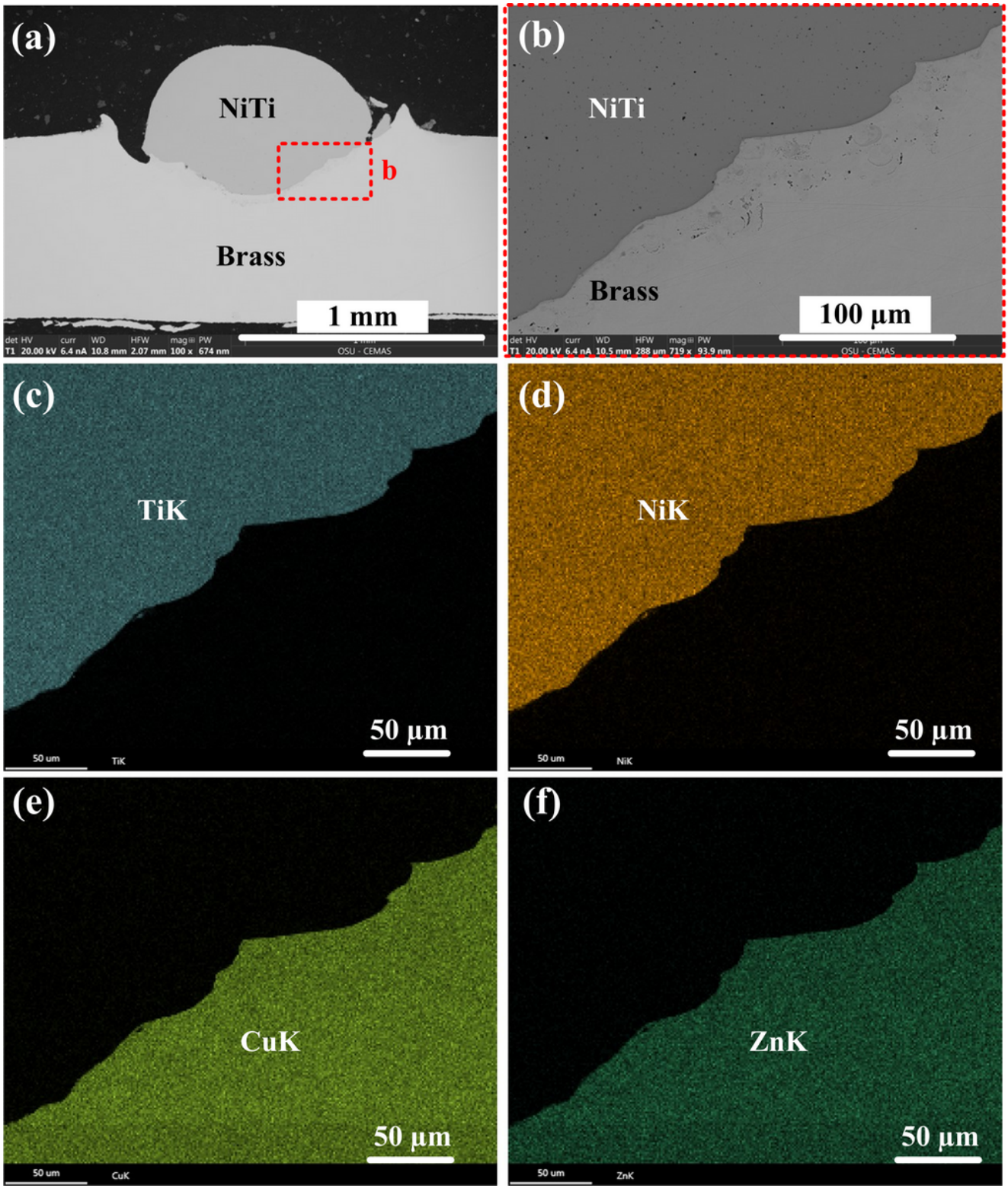

Figure 4

Interfacial microstructures and EDS mapping analyses of a typical NiTi/Brass weld. (a) Cross-section overview of the NiTi/Brass weld; (b) An enlarged view of a wavy interface in dashed square area in (a); (c) Elemental distribution map of TiK of the wavy interface in (b); (d) Elemental distribution map of NiK of the wavy interface; (e)Elemental distribution map of CuK of the wavy interface; (f) Elemental distribution map of ZnK of the wavy interface.

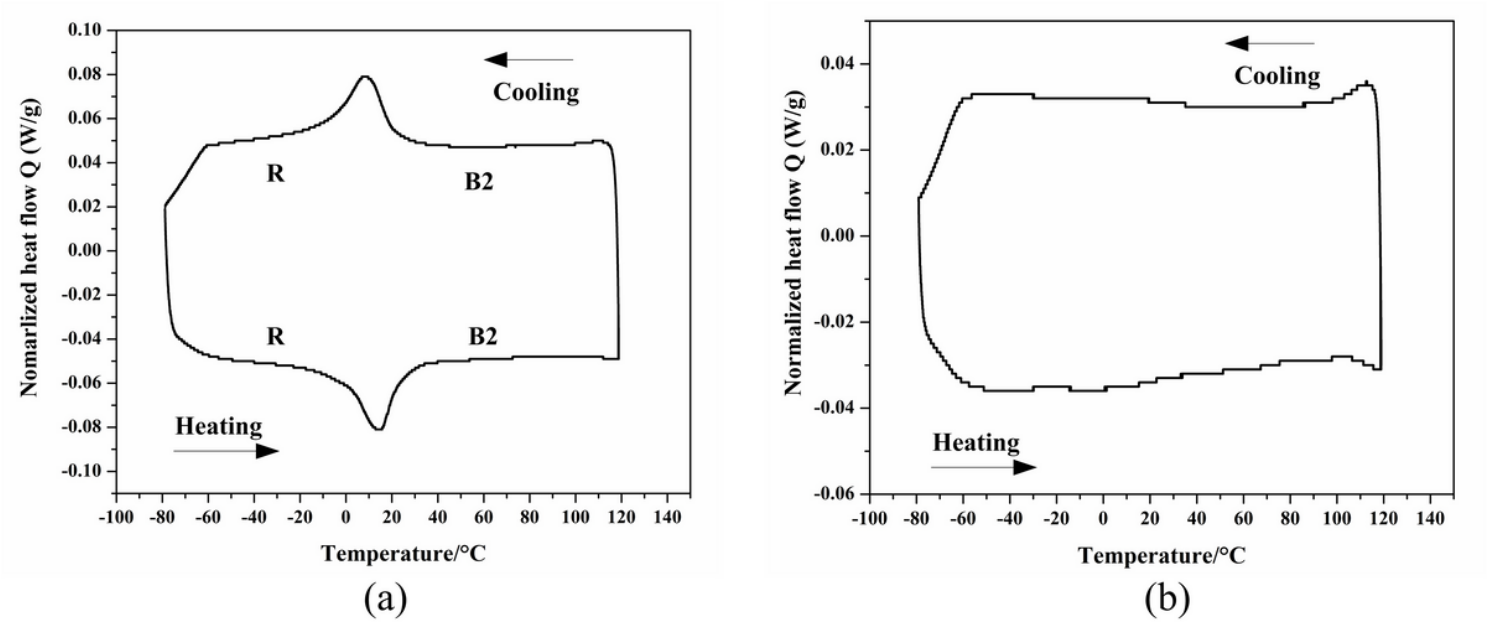

Figure 5

Comparison of differential scanning calorimetry (DSC) testing results between NiTi base metal (BM) in (a), and NiTi/Brass weld in (b).

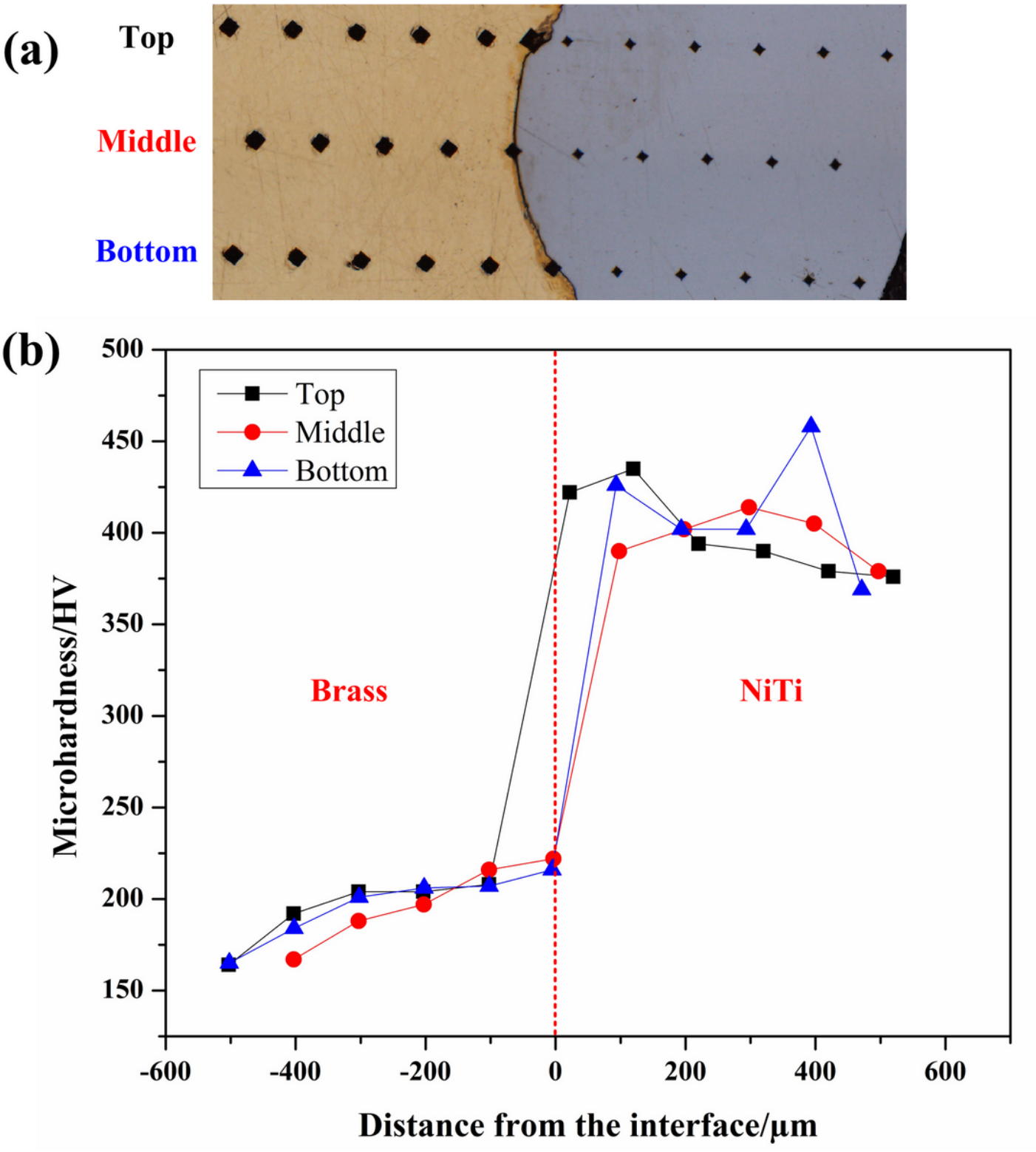

Figure 6

Microhardness distribution across the interface of NiTi/Brass weld. (a) Microhardness measurement locations across the interface; (b) Microhardness distribution versus distance from the interface.

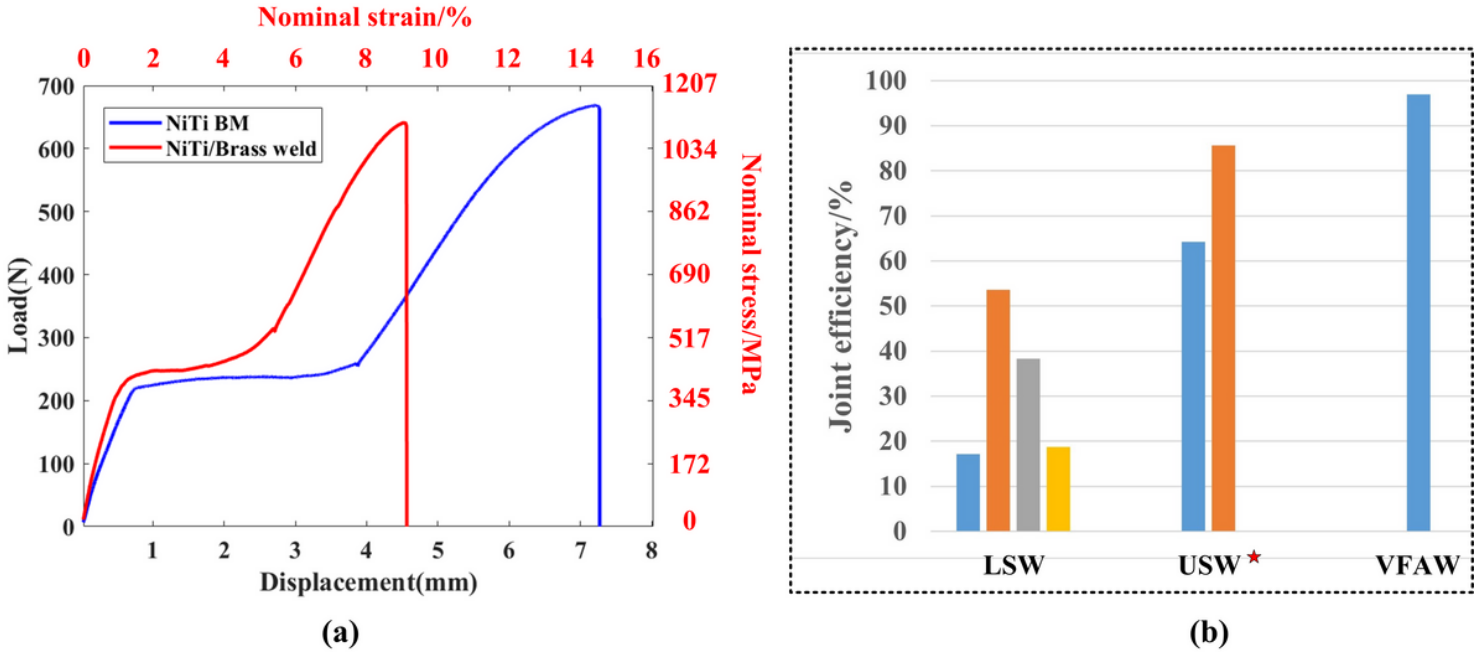

Figure 7

(a) Comparison of lap shear testing results between NiTi BM and NiTi/Brass weld; (b) Comparison of joint efficiencies among laser welding (LSW), ultrasonic spot welding (USW), and VFAW in the current work. The red asterisk signifies that USW only works on very thin foils and has not been applied to weld stiff NiTi wires.

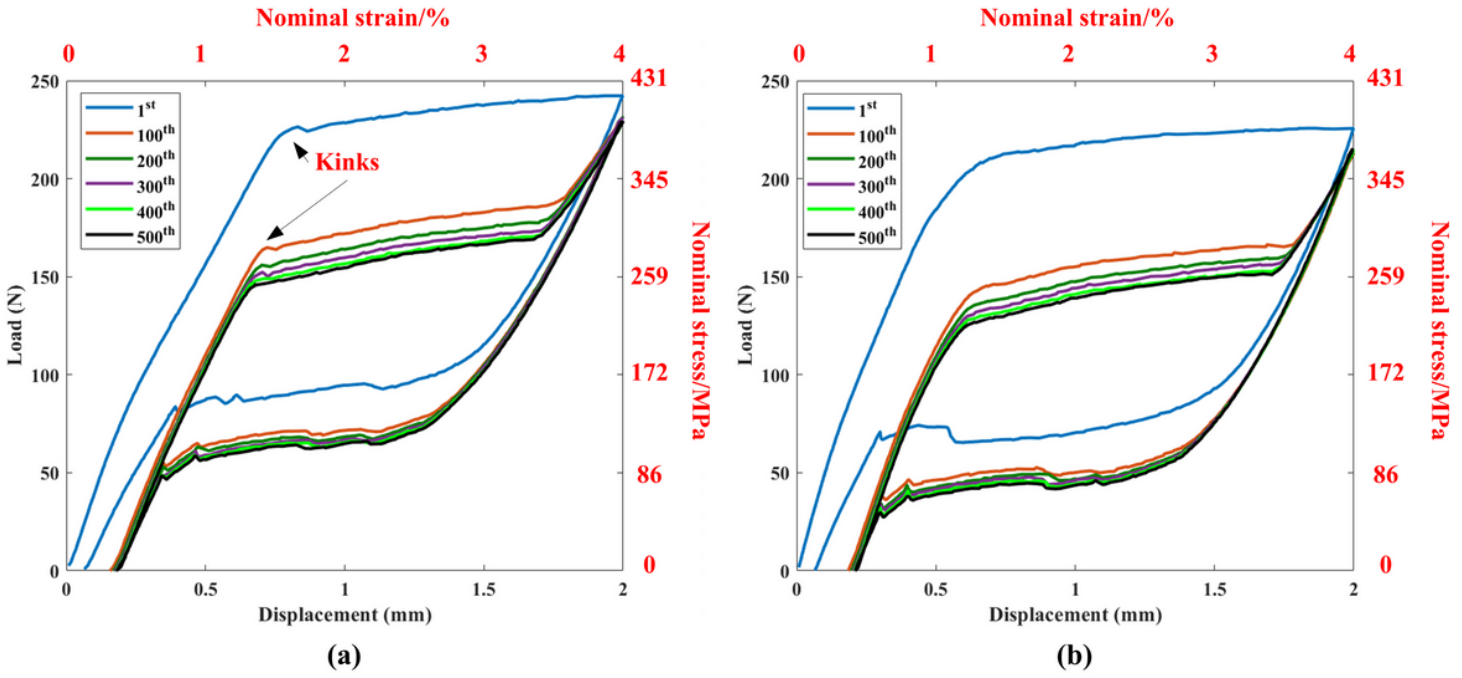

Figure 8

Comparison of cycling test results between NiTi BM in (a) and NiTi/Brass weld in (b) after 500 cycles. The 1st, 100th, 200th, 300th, 400th, and 500th cycles were singled out and represented in different colors.

The weld is being strained to twice the amount as the base metal because only half of the gauge length is NiTi.